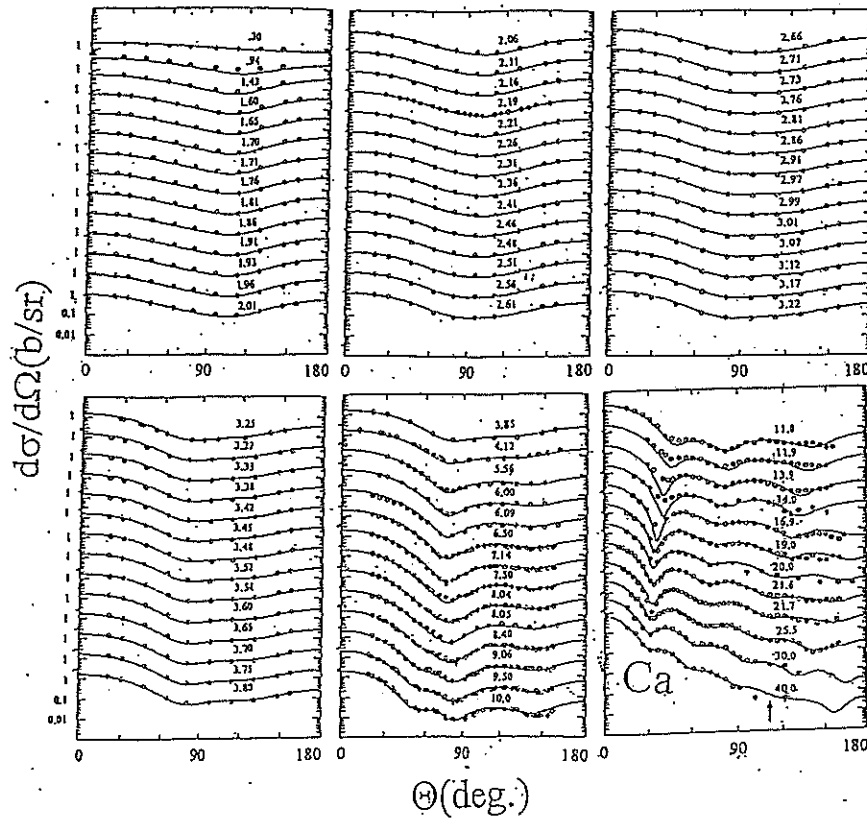


Fast Neutrons, Calcium, Models and Potentials

Nuclear Data and Measurement Series

by:- Alan B. Smith
Nuclear Engineering Division



About Argonne National Laboratory

Argonne is a U. S. Department of Energy laboratory managed by UChicago Argonne LLC, under contract DE-AC02-06CH11357. The Laboratory's main facility is outside Chicago, at 9700 South Cass Avenue, Argonne, Illinois 60439, USA. For information about Argonne see www.anl.gov.

Availability of this report

This report is available, at no cost, at <http://www.osti.gov/bridge>. It is also available on paper to the U. S. Department of Energy and its contractors, from the

U. S. Department of Energy
Office of Scientific and Technical Information
P.O. Box 62
Oak Ridge, TN 37831-0062
Phone (865)576-8401
Fax (865) 576-5728

Disclaimer

This report was prepared as an account of work sponsored by an agency of the United States Government. Neither the United States Government nor any agency thereof, nor UChicago Argonne LLC nor any of their employees or officers, make any warranty, expressed or implied, or assumes any legal liability or responsibility for the accuracy, completeness, or usefulness of any information, apparatus, product, or process disclosed, or represents that its use would not infringe on privately owned rights. Reference herein to any specific commercial product, process, or service by trade name, trademark, manufacturer, or otherwise, does not necessarily constitute or imply its endorsement, recommendation or favoring by the United States Government or any agency thereof. The views and opinions of the documents author(s) expressed herein do not necessarily state or reflect those of the United States Government or any agency thereof, Argonne National Laboratory, or UChicago Argonne LLC.

Nuclear Data and Measurement Series

Reports in the Argonne National Laboratory Nuclear Data and Measurement Series present results of studies in the field of microscopic nuclear data. The primary objective of the series is the dissemination of information in the comprehensive form required for nuclear technology applications. This series is devoted to a) measured microscopic nuclear parameters, b) experimental techniques and facilities employed in measurements, c) the analysis, correlation and interpretation of nuclear data, and d) the compilation and evaluation of nuclear data. Contributions to this series are reviewed to assure technical competence and, unless otherwise stated, the contents can be formally referenced. This series does not supplant formal journal publication, but it does provide the more extensive information required for technological applications (e.g. tabulated numerical data) in a timely manner.

Other Publications in the ANL/NDM Series

A listing of recent issues in this series is given below. Issues and/or titles prior to ANL/NDM-130 can be obtained from the National Technical Information Service, U.S. Department of Commerce, Technology Administration, Springfield, VA 22161, or by contacting the authors of this report at the Nuclear Engineering Division, Argonne National Laboratory, Argonne IL 60439 (USA). In addition, the entire report series can be found on the Internet at the following LRL:-

<http://www.ne.anl.gov/capabilities/nd/reports/index.html>,

or under ANL/NDM using any internet search engine such as "GOOGLE", including abstracts, complete reports, and associated computer programs.

- A. B. Smith and P. T. Guenther
Fast-neutron interaction with the fission product ^{103}Rh
ANL/NDM-130, September 1993
- A. B. Smith and P. T. Guenther
Fast-neutron scattering from vibrational Palladium nuclei
ANL/NDM-131, October 1993
- A. B. Smith
Neutron interaction with doubly magic ^{40}Ca
ANL/NDM-132, November 1993
- A. B. Smith
Neutron scattering at $Z \approx 50$:- Tin
ANL/NDM-133, September 1994
- A. B. Smith, S. Chiba (JAERI) and J. Meadows
An evaluated neutronic data file for elemental Zirconium
ANL/NDM-134, September 1994

- A. B. Smith and S. Chiba (JAERI)
Neutron scattering from Uranium and Thorium
ANL/NDM-135, February 1995
- A. B. Smith
Neutron scattering and models:- Iron
ANL/NDM-136, August 1995
- A. B. Smith
Neutron scattering and models:- Silver
ANL/NDM-137, July 1996
- A. B. Smith and D. Schmidt (PTB)
Neutron scattering and models:- Chromium
ANL/NDM-138, June 1996
- W. P. Poenitz and S. E. Aumeier
The simultaneous evaluation of the standards and other cross sections
of importance for technology
ANL/NDM-139, September 1997
- D. L. Smith and J. T. Daly
A compilation of information on the $^{31}\text{P}(p,\gamma)^{32}\text{S}$ reaction and properties of excited
levels in ^{32}S
ANL/NDM-140, November 2000
- A. B. Smith
Neutron scattering and models:- Titanium
ANL/NDM-141, July 1997
- A. B. Smith
Neutron scattering and models:- Molybdenum
ANL/NDM-142, July 1999
- R. E. Miller and D. L. Smith
Compilation of information on the $^{31}\text{P}(p,\gamma)^{33}\text{Cl}$ reaction and properties of
excited levels in ^{33}Cl
ANL/NDM-143, July 1997
- R. E. Miller and D. L. Smith
A compilation of information on the $^{31}\text{P}(p,\gamma)^{28}\text{Si}$ reaction and properties of
excited levels in ^{28}Si
ANL/NDM-144, November 1997
- R. D. Lawson and A. B. Smith
ABAREX, a neutron optical-statistical model code. A user's manual
ANL/NDM-145, June 1999
- R. T. Klann and W. P. Poenitz
Non-destructive assay of EBR-II blanket elements using resonance transmission
analysis
ANL/NDM-146, August 1998
- A. B. Smith
ELEMENTAL-ABAREX:- a user's manual
ANL/NDM-147, June 1999

- D. G. Naberejnev and D. L. Smith
A method to construct covariance files in ENDF/B formats for critical safety applications
ANL/NDM-148, June 1999
- A. B. Smith
Neutrons and antimony, physical measurements and interpretations
ANL/NDM-149, July 2000
- A. B. Smith and A. Fessler
Neutrons and antimony, neutronic evaluations of ^{121}Sb and ^{123}Sb
ANL/NDM-150, July 2000
- A. B. Smith
Fast neutrons incident on Holmium
ANL/NDM-151, December 2000
- R. D. Lawson and A. B. Smith
Technical note:- dispersion contributions to neutron reactions
ANL/NDM-152, August 2001
- A. B. Smith
Fast neutrons incident on Hafnium
ANL/NDM-153, June 2001
- D. L. Smith, Dimitri G. Naberejnev and L. A. Van Wormer
An approach for dealing with large errors
ANL/NDM-154, September 2001
- A. B. Smith
Fast neutron scattering from elemental Rhenium
ANL/NDM-155, August 2003
- D. L. Smith
A demonstration of the lognormal distribution
ANL/NDM-156, July 2003
- A. B. Smith
Fast neutrons incident on Gadolinium
ANL/NDM-157, April 2004
- D. L. Smith
A survey of experimental and evaluated fast-neutron Helium production data for fission applications
ANL/NDM-158, May 2004
- D. L. Smith
Covariance matrices for nuclear cross sections derived from nuclear models
ANL/NDM-159, January 2005
- A. B. Smith
Fast-neutrons incident on rotors:- Tantalum
ANL/NDM-160, February 2005
- A. B. Smith
Neutron scattering from the standard ^{197}Au
ANL/NDM-161, June 2005

F. Kondev

Evaluated decay data for ^{206}Tl
ANL/NDM-162, November 2006

A. B. Smith

Remark on the neutron spherical optical-model absorption
ANL/NDM-163, August 2007

F. Kondev

Evaluated decay data for ^{246}Cm
ANL/NDM-164, November 2006

A. B. Smith

Fast neutrons, Calcium, Models and Potentials
ANL/NDM-165, December 2010

D. L. Smith

A unified Monte-Carlo approach to fast-neutron cross section evaluation
ANL/NDM-166, January 2008

Fast Neutrons, Calcium, Models and Potentials

Nuclear Data and Measurement Series

by

Alan B. Smith

Nuclear Engineering Division, Argonne National Laboratory
The Physics Consultative, Ottawa, Illinois

Keywords:- Fast neutrons incident on doubly-magic, iso-spin zero, Ca-40 are considered. Comparisons of experimental and evaluated quantities and, spherical and vibrational model predictions are discussed. An energy dependent asymmetric shape of the surface-imaginary absorption is proposed.

Abstract

The experimental neutron cross sections of elemental Calcium were assembled from the world data centers up to incident-neutron energies of ≈ 50 MeV. These results were interpreted in terms of spherical optical and vibrational coupled-channels models, assuming elemental Calcium is essentially the isotope Ca-40, doubly magic with equal numbers of neutrons and protons (20) and thus has zero iso-spin. The model results are compared with various evaluated files and with the predictions of the calculational systems widely used in evaluations.



UChicago 
Argonne_{LLC}



A.U.S. Department of Energy laboratory managed by UChicago Argonne, LLC

I. Introductory Comment

More than half a century ago A. Lane et al. (Lan+59) pointed out that observed neutron-nucleus interactions are sensitive to nuclear structure, in particular to nuclear shell structure. This structure is superimposed on broader-ranging isospin ($T=(N-Z)/A$) and giant-resonance effects which are minimum near shell closures, and some, by definition, zero at the doubly closed shell where $T=0$. This extreme case should be approached in ^{40}Ca which is the heaviest naturally occurring $T=0$ isotope, and which makes up approximately 97% of elemental Calcium. Early on, observed strength functions were shown inconsistent with the strong coupling model and with the common surface and volume absorption optical model. Moreover, observed neutron reactions with ^{40}Ca were not well described, particularly at incident neutron energies near 10 - 20 MeV (e.g. Hon+86, Tor+82). A number of model artifices have been examined to alleviate the discrepancies between measurements and model prediction; e.g. dispersive effects, geometric factors, asymmetric $[(N-Z)/A]$ potential terms, l -dependent potentials, and coupling with a giant resonance (Hon+86, Tor+82, Pig+81), all without pronounced success. There is some model sensitivity to shell structure near proton and/or neutron numbers 50, 82 and 126, but the magnitude is greater with the $T = 0$ target ^{40}Ca . One would expect the surface imaginary potential to be quite small and symmetric about the imaginary-potential radius at low energies but with increasing incident energy it should spread asymmetrically toward the interior of the nucleus with increasing overall strength. Such trends have been observed in neutron scattering from targets near neutron number $N=50$ (Zr and Nb) and proton number $P=82$ (Pb and Bi, (Smi07)). The effects should be much more acute with the $T=0$ ^{40}Ca . They are often approximated by introducing an energy dependent volume-imaginary potential, with only modest success.

II. Experimental Foundation

II.1. Neutron energy-averaged total cross sections

All of the Ca and ^{40}Ca experimental neutron total cross sections available at the National Nuclear Data Center (NNDC) were assembled into one large data set, irrespective of experimental energy resolutions. This data set was graphically inspected and a few obviously erroneous values rejected. It then consisted of over 25,000 differential values extending from essentially zero energy to ≈ 600 MeV, and largely consisted of several large white-source data sets. It was ordered by energy with the results illustrated in Fig. II.1.A. Below ≈ 5 MeV it is clearly characterized by isolated resonance structure. The agreement between the various data sets is remarkably good given the inevitable variations in experimental energy scales and resolutions. At higher energies the measurements blend into an energy-averaged behavior, but it is clear there are several data sets that drift off the general energy dependence. These were identified

graphically and culled from the master set. Of course, there remain large resonance fluctuations at low energies. Therefore, this large master set was energy averaged over ≈ 50 keV intervals below 0.5 MeV, over ≈ 100 keV intervals from 0.5 to 5.0 MeV, and over ≈ 200 keV intervals at higher energies in order to provide energy-averaged values consistent with the model concepts discussed below. The resulting energy-averaged total cross sections are illustrated in **Fig. II.1.B** over the 0-40 MeV range consistent with the available scattering measurements outlined below. Above approximately 5 MeV the averaged total cross sections are a reasonably smooth function of energy. However, below ≈ 5.0 MeV the underlying resonance structure remains evident even in the relatively broad energy average. These experimentally based total cross sections are consistent with ENDF/B-VII as indicated by the comparisons of **Figs. II.1.C** and **II.1.D**.

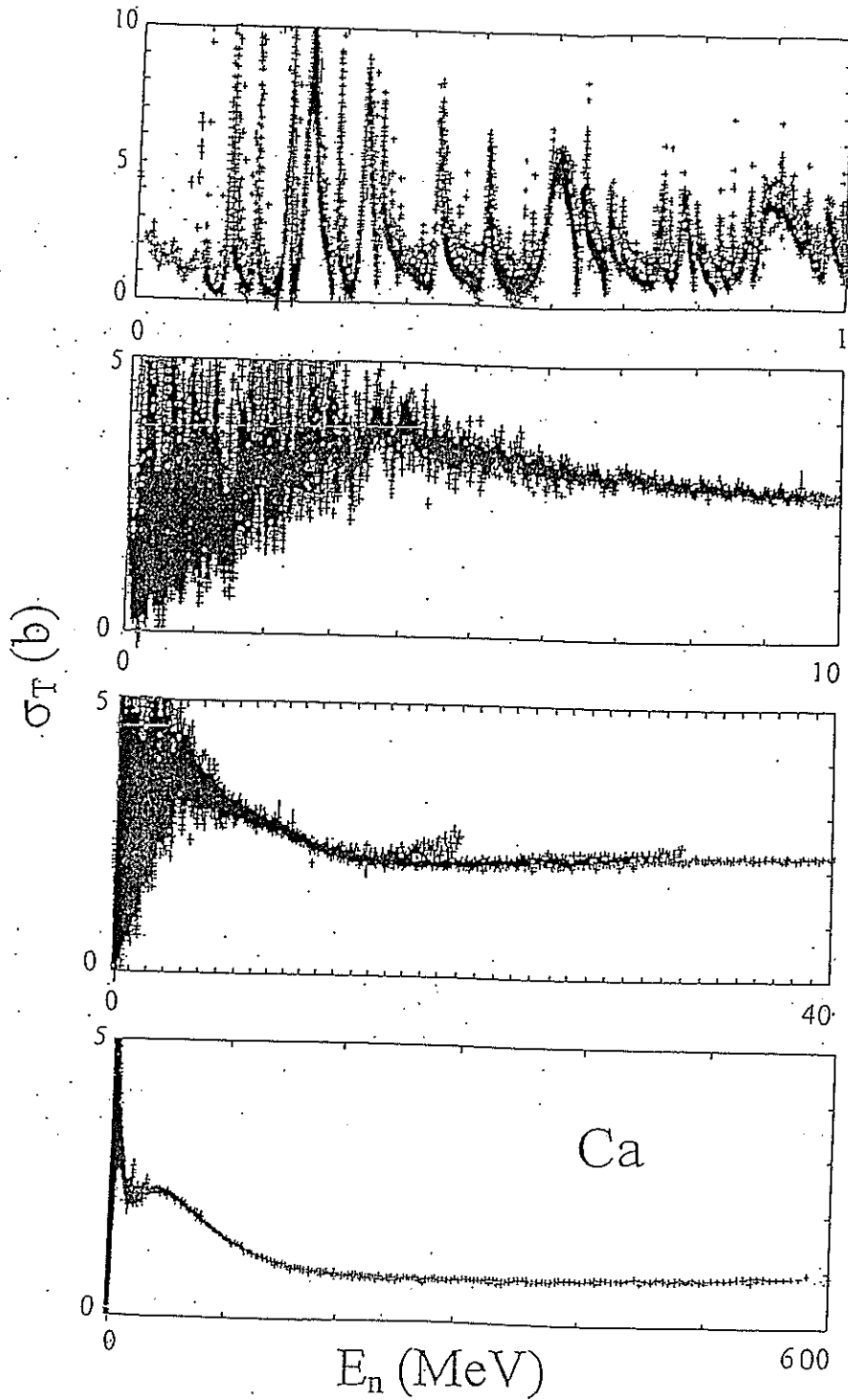


Fig. II.1.A. Experimental Calcium neutron total cross sections as reported in the literature and described in the text. There are more than 25000 values which were ordered by energy and plotted. There are clearly some discrepant data sets.

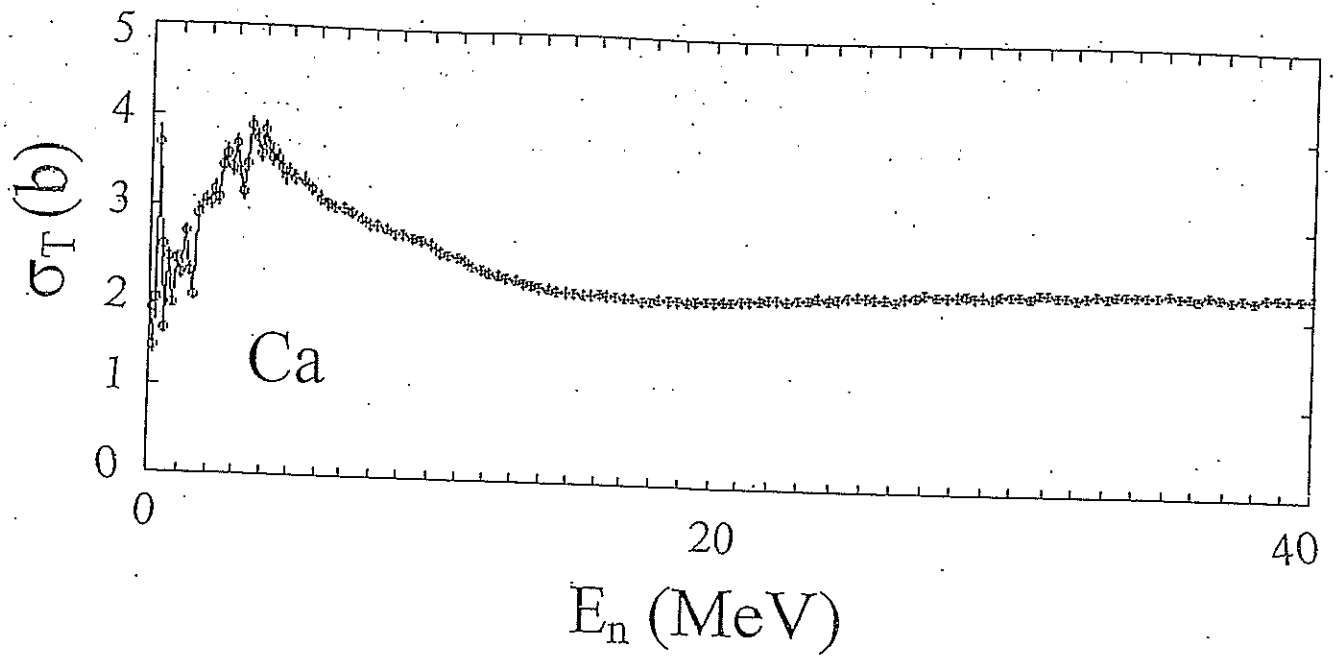


Fig. II.1.B. Ordered, culled and averaged experimental neutron total cross sections of Calcium derived as described in the text. The individual average values are indicated by circular symbols which are joined by the solid curve.

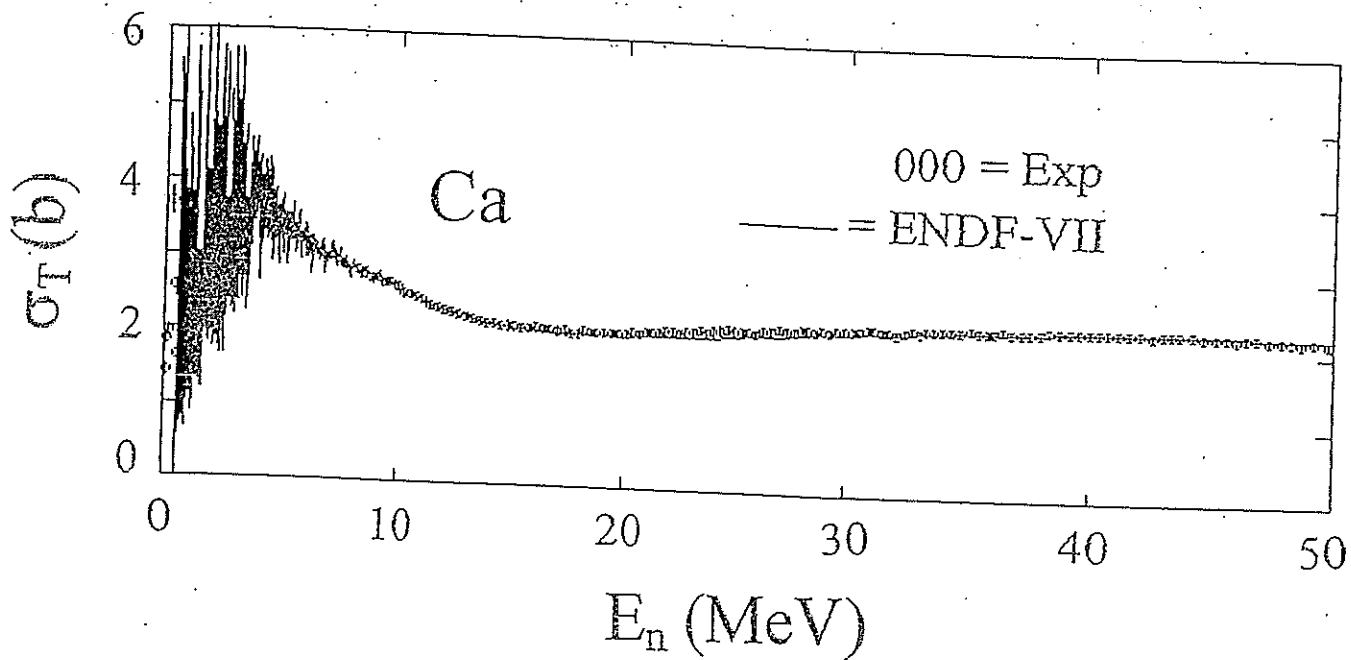


Fig. II.1.C. Comparison of the present energy-averaged total cross sections (circular symbols) and ENDF/B-VII total cross sections (curve) to 50 MeV.

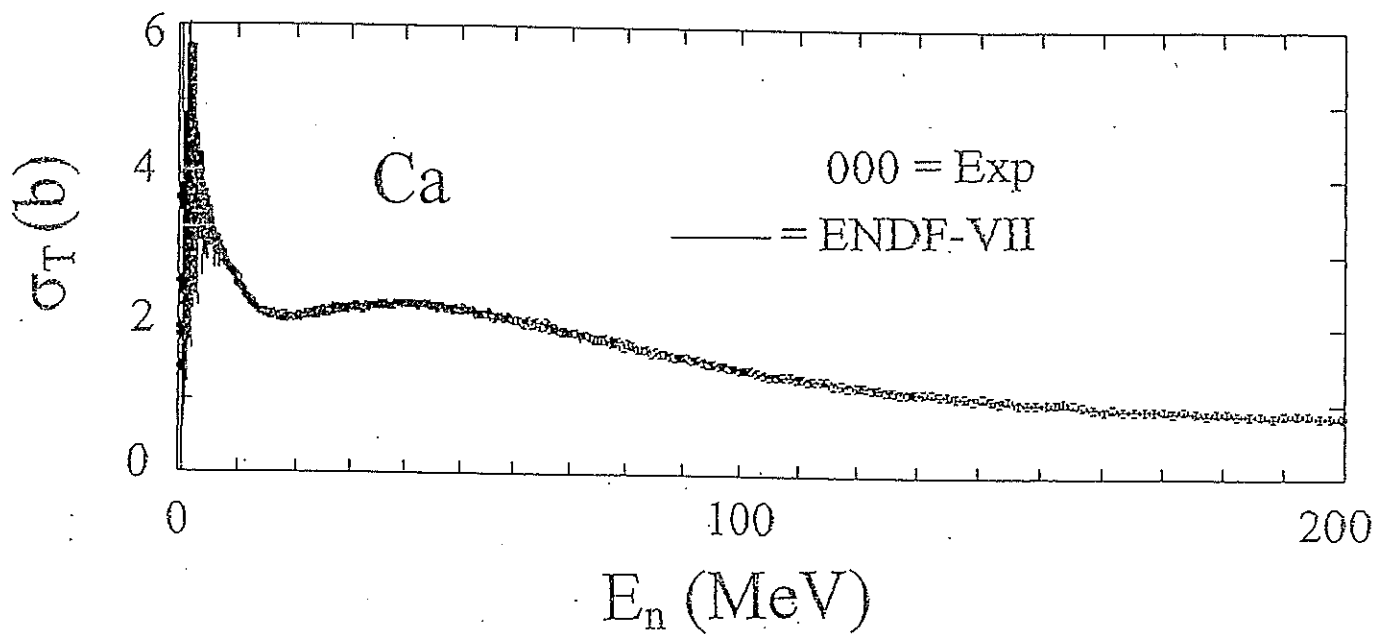


Fig. II.1.D. Comparisons of Fig.II.1.C extended to 200 MeV.

II.2 Neutron energy-averaged elastic scattering

The files of the National Nuclear Data Center (NNDC) were also searched for the experimental neutron elastic-scattering data of elemental Ca and ^{40}Ca at incident energies above ≈ 30 keV. That database was graphically culled and data from the following 24 references accepted for model interpretation.

Accepted References

1. R. Lane et al., *Annals Physics* 12 135 (1961) #10415
 2. J. Seagrave et al., *Phys. Rev.* 119 60 (1961) #11620
 3. D. Abramson et al., Report EANDC(E)-149 (1971) #20512
 4. A. Smith, *Nucl. Phys. A* 576 165 (1994) #12749B
 5. J. Reber and J. Brandenberger, *Phys. Rev.* 163 1077 (1967) #11618
 6. S. Hicks, Priv. Com., to NNDC (1988) #13508
 7. D. Winterhalter, *Ziets. Phys.* 200 487 (1967) #30201
 8. V. Popov, *Neutronfiz* 306 (1961) #41215
 9. R. Becker et al., *Nucl. Phys.* 89 154 (1966) #11511
 10. D. Kent et al., *Phys. Rev.* 125 331 (1962) #11617
 11. B. Holmqvist et al., Report AE-366 (1969) #20019
 12. J. Ferrer et al., *Nucl. Phys. A* 275 325 (1977) #10633
 13. W. Tronow et al., *Nucl. Phys. A* 385 373 (1982) #12785
 14. G. Honore et al., *Phys. Rev. C* 33 1129 (1986) #12996
 15. A. Frasca et al., *Phys. Rev.* 144 854 (1968) #10254
 16. J. Rapaport et al., *Nucl. Phys. A* 462 413 (1987) #13127
 17. J. Rapaport et al., *Nucl. Phys. A* 286 232 (1977) #10697
 18. N. Olsson et al., *Nucl. Phys. A* 472 237 (1987) #22048
 19. R. DeVito et al., *Phys. Rev. Lett.* 47 628 (1981) #12724
 20. A. Smith and P. Guenther, Argonne Natl. Lab. Report ANL/NDM-65 (1982).
 21. A. Smith, Argonne Natl. Lab. Report ANL/NDM-132 (1993).
 22. F. Perey et al., Oak Ridge Natl. Lab. Report ORNL-4519 (1970) #10109
 23. W. Cross et al., *Nucl. Phys.* 15 155 1960 #11465
 24. J. Weddell, *Phys. Rev.* 104 1069 1965 #11615
- # herein denotes NNDC-BNL acquisition number

This data extends from ≈ 30 keV to 40.3 MeV. Lower energy data was ignored as it was sparse and dominated by isolated resonances. There are a few additional higher-energy distributions ((Os+04) and (Hjo+45)) extending up to as high as incident energies of 95 MeV, but the data is all at very forward scattering angles and thus not suitable for the present considerations. This broad-resolution elastic-scattering data base was subjectively energy averaged over \approx several-hundred keV intervals below 10 MeV using Legendre fitting procedures in order to smooth any remaining resonance fluctuations. At higher energies the distributions were accepted as reported by the various authors. The resulting energy averaged elastic-scattering distributions are illustrated in **Fig. II.2.A**. In this figure, circular symbols indicate values deduced from the measurements, while curves are eye-guides following from Potential 93, below.

Considerations of comparisons with other model predictions are a primary thrust of the discussion elsewhere herein.

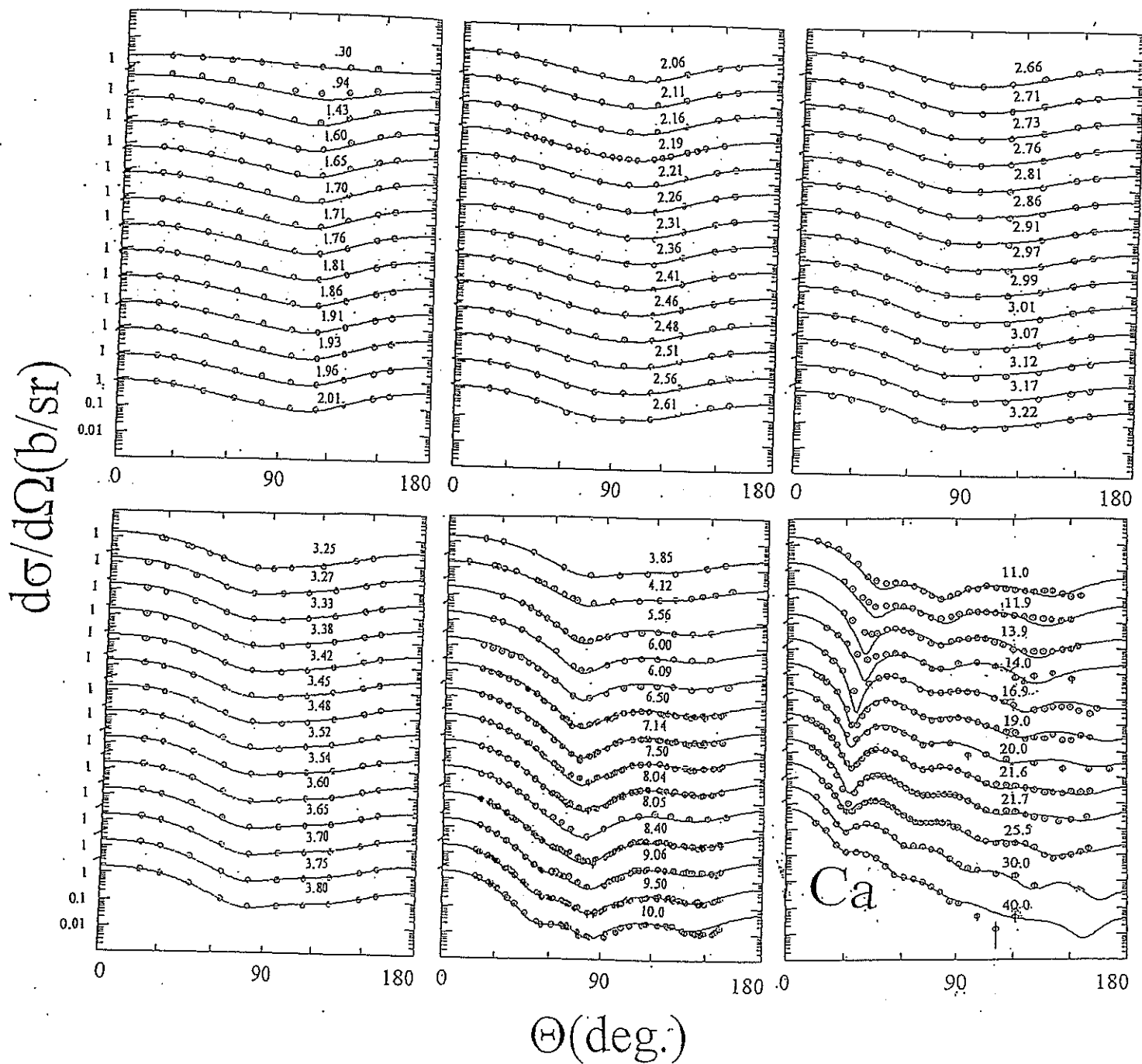


Fig. II.2.A. Illustrative energy-averaged Ca elastic-scattering distributions. Energy-averaged experimental values are indicated by circular symbols. Curves illustrate the results of model calculations using the Potential 93 cited in the text. Incident energies are numerically indicated in MeV. Curves are offset in energy by an order of magnitude.

The energy averaged elastic angle integrated experimental cross sections are remarkably consistent with the values given in ENDF/B-VII, as shown in the upper portion of **Fig. II.2.B**. Below approximately 6 MeV the evaluated elastic scattering is described by large resonance structure. However, the average magnitude of this low lying structure is reasonably consistent with the results of the broader-resolution elastic-scattering measurements as shown by the energy-averaged comparisons of the lower portion of the figure.

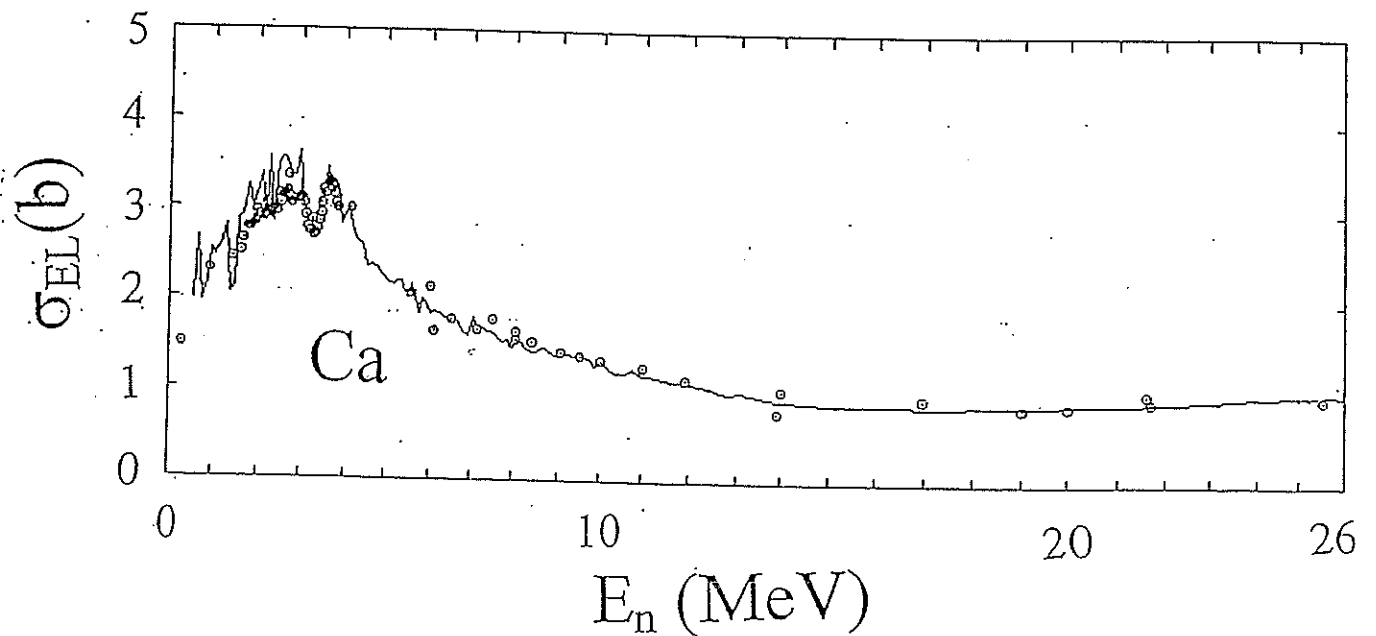
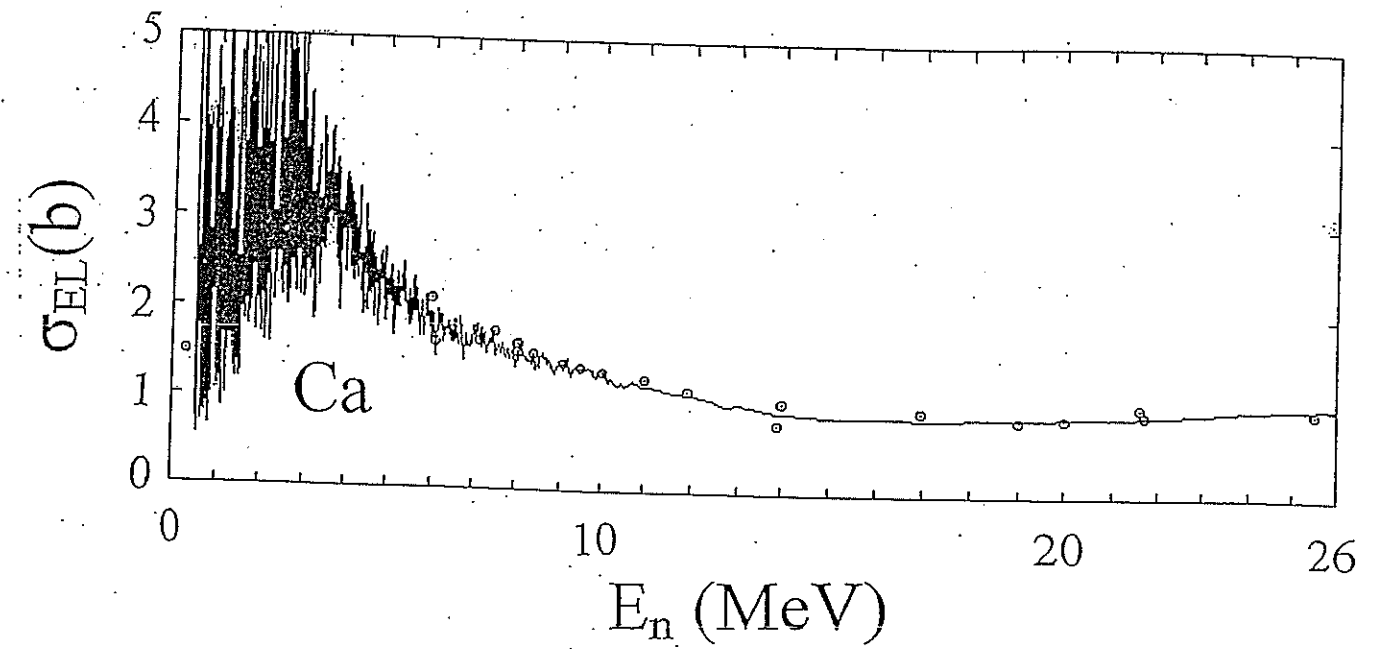


Fig. II.2.B. Comparisons of energy averaged experimental Ca elastic scattering cross sections (symbols) with the Ca ENDF/B-VII elastic scattering evaluation (curve). The ENDF results are not averaged in the upper panel, but in the lower panel they are averaged by an energy interval qualitatively equivalent to that used for the measurements.

II.3 High resolution elastic-scattering measurements

An additional reference (Toe74) was examined in detail. It consists of white-source high-resolution differential elastic distributions measured every few keV from approximately 1.0 to 6.0 MeV. The resolution is excellent and the definition of the elastic scattering within the resonance region is very good. This unusual data set was fitted with Legendre polynomial expansions from which the angle integrated elastic scattering cross sections were derived. Unfortunately, with increasing energy it appears that the energy-averaged magnitude of the distributions increasingly exceeds that indicated by the broader-resolution measurements outlined above. Thus these high-resolution scattering results appear inconsistent with the broader-resolution experimental results and were not considered in the present physical interpretations.

II.4 Other neutron-induced particle emission

The (n,p) and (n, α) reaction channels of ^{40}Ca are abnormally large, collectively approaching a barn below incident energies of approximately 10 MeV. For the present interpretations the ((n,p) + (n, α)) values given in ENDF/B-VII were used as described in the model discussion below. Corresponding but fragmentary experimental information is available at the National Nuclear Data Center which reasonably supports the ENDF/B-VII evaluation (which may well be a model estimate) used here.

II.5 Inelastic neutron scattering measurements

The inelastic neutron scattering is assumed to be entirely due to Ca-40(98% elemental abundance, iso-spin=0.0). Level properties were taken from J. Cameron and B. Singh, (Nucl. Data Sheets 102, 293 (2004)) and P. Endt and C. Van de Leun (Nucl. Phys A310, 561 (1978)). Thirteen levels were assumed up to excitations of 6.029 MeV. Their excitation energies, spins and parities are summarized in **TABLE II.5.1**. Higher-energy excitations were treated as a continuum distribution of levels using the parameterization of A. Gilbert and A. Cameron (GC65).

TABLE II.5.1. Assumed C-40 levels

Number,	Excitation (MeV),	Spin,	Parity
1	0.0	0.0	+1
2	3.352	0.0	+1
3	3.736	3.0	-1
4	3.904	2.0	+1
5	4.491	5.0	-1
6	5.211	0.0	+1
7	5.244	2.0	+1
8	5.279	4.0	+1
9	5.613	4.0	-1
10	5.629	2.0	+1
11	5.903	1.0	-1
12	6.025	2.0	-1
13	6.029	3.0	+1

Illustrative accepted inelastic-scattering references.

1. F. Perey and W. Kinney, Oak Ridge Natl. Lab. Report, ORNL-4519 (1970) #10109
 2. A. Smith, Argonne Natl. Lab. Report, ANL/NDM-132 (1993) #12749
 3. C. Bartle and P. Quin, Ann. Nucl. En., 8, 43 (1981) #10447
 4. D. Bainum et al., Phys., Rev. C16 1377 (1977) #10699
 5. W. Tornow et al., Nucl. Phys. A385 373 (1982) #12785
 6. G. Honore et al., Phys. Rev. C33 1129 (1986) #12996
 7. R. Alarcon and J. Rapaport, Nucl. Phy. A462 445 (1987) #13126
 8. S. Hicks et al., Phys. Rev. C41 2560 (1990) #13507, #13508
 9. N. Olsson et al., Nucl. Phys. A513 205 (1990) #22128
 10. O. Sal Nikov et al., JYF 4 1154 (1966) #40134
 11. R. Day, Phys. Rev. 102 762 (1956) #11218
- # denotes NNDC-BNL acquisition number

III. Model Interpretations.

III.1. A basic spherical optical model (SOM)

All of the present spherical optical model interpretations employed various versions of the neutron spherical optical-model code ABAREX (LS99). The basic version will handle dispersion effects using the approximations of Lawson and Smith (LS01), as discussed in title III.3, below. Another version called ANLCN has a provision for introducing an additional compound nucleus component. In the case of ^{40}Ca this contribution was attributed to the sum of (n, α) and (n,p) reactions, assuming they were compound-nucleus processes. The neutron elastic and inelastic scattering

compound-nucleus contributions were then adjusted to be consistent with the remainder of the compound nucleus components. Such compound-nucleus contributions are usually quite small at lower incident energies (e.g. fast neutron capture) and ignored in routine optical and statistical model interpretations. For ^{40}Ca the (n, α) and (n,p) contributions are significant from several 100 keV to above several MeV. At higher energies there are many open neutron and other compound nucleus channels and, as a consequence, compound-neutron emission to each channel is negligible as described in Section III.2 and should receive attention as outline below. The ABACN model will adjust the compound nucleus distribution accordingly. More complex particle emission mechanisms will alter this simple compound-nucleus-emission picture. The underlying optical-model potential form is conventional and well defined in the literature for more than half a century (Hod63, OR82, Elt61, Rap82, Gpt68, and others). The potential consists of a real volume term, imaginary surface and volume terms, and a real spin-orbit term, and takes the form:-

$$V(r) = U f(r_u) + i [W_v f(r_{vs}) + W_s g(r_{ws})] + U_{so} (h/\mu\pi c)^2 (1/r_{so}) d/dr_{so} [f_{so}(r_{so})] \sigma \cdot l, \quad \text{III.1.A,}$$

where U = real-potential depth, W_v = the volume-imaginary depth, W_s = the surface imaginary depth, U_{so} = the real spin-orbit depth. $f(r_i)$ is taken to be the Saxon-Woods form

$$f(r_i) = 1/[1 + \exp((r_i - R_i)/a_i)] \quad \text{III.1.B}$$

and $g(r)$ to be of the Saxon-Woods-derivative form

$$g(r_i) = -4 b_w d/dr [(1 + \exp((r_i - R_w)/b_w))^{-1}], \quad \text{III.1.C}$$

or thus

$$g(r_i) = 4 \exp((r_i - R_w)/b_w) / (1 + \exp((r_i - R_w)/b_w))^2, \quad \text{III.1.D}$$

where r_i = the reduced real radius, a_U = the real diffuseness, the real radius $R_U = r_U \cdot A^{1/3}$ (where A = the target mass in AMU), the imaginary radius $R_w = r_w \cdot A^{1/3}$, where r_w is the reduced imaginary radius, and b_w = the imaginary diffuseness. As will become clear in the following considerations, W_v is set identically to zero throughout the present considerations unless otherwise explicitly stated. The spin-orbit term is of the Thomas form and real (no imaginary spin-orbit component). Real and imaginary potential-integrals-per-nucleon are (see refs. Elt61, Ols+82, Hod63, and/or Rap82),

$$J_U/A = (4/3) \pi (R_U^3/A) U [1 + (\pi a_U/R_U)^2] \quad \text{III.1.E}$$

$$J_w/A = 16(\pi R_w/A)^2 b_w W [1 + (1/3) ((\pi b_w)/R_w)^2] \quad \text{III.1.F}$$

The real and imaginary RMS radii are

$$\langle R_U^2 \rangle^{1/2} = [(3 R_U^2 + 7 \pi^2 a_U^2)/5]^{1/2} \quad \text{III.1.G}$$

$$\langle R_W^2 \rangle^{1/2} = \{ 12 b_W R_W [1 + (\pi b / R_W)^2] (J_U^0 / J_W^0) \}^{1/2}, \quad \text{III.1.H}$$

where J_U^0 and J_W^0 are the values given by Eqs. III.1.E and III.1.F with $U = W = 1$.

Conventionally, the imaginary potential widths given by Eqs. III-1.C and III-1.D are taken to be symmetric about r_W , and if a volume absorption is desired it is introduced as a separate W_V which is usually energy dependent. Here the concept of an asymmetric imaginary diffuseness is introduced, where b_W may have different values (b_{Wi}) interior-to and (b_{Wo}) exterior-to the imaginary radius r_W . This asymmetry of the surface absorption potential is here defined as

$$\text{ASYM} = 1 + K \cdot E, \quad \text{III.1.I}$$

where "K" is a constant and $b_{Wi} = \text{ASYM} \cdot b_{Wo}$. This concept provides for a progressive linear growth of the surface absorption into the interior of the nucleus with incident energy (i.e. surface absorption changing to volume absorption with energy). Eq. III.1.I is a simple linear approximation describing such an effect. Of course, more complex energy dependencies can be introduced, This transition in shape of the surface absorption with K is illustrated by the relative distributions shown in Fig. III.1.1. The concept replaces a minimum of five parameters associated with parameterizations using the conventional volume absorption potential (strength, radius, diffuseness, energy dependence and threshold) with the single parameter "K". This is a prominent advantage in the use of an optical potential already overloaded with parameters.

Comparisons of results obtained with appreciably different target masses should always be cognizant of iso-spin effects where $V = V_0 \pm \eta V_1$, $W = W_0 \pm \eta W_1$, ("+" for protons and "-" for neutrons) and $\eta = (N-Z)/A$ (Lan62). However, the present considerations are largely confined to the neutron interaction with Ca-40 which is the heaviest doubly-magic nucleus of large natural abundance in the periodic table. Therefore, the iso-spin effects are not explicit considerations in the present work.

The above rudimentary spherical model does not consider dispersive contributions which fundamentally couple real and imaginary potentials (Sat83), as discussed elsewhere in this note. The above remarks also do not address collective effects and the associated deformations and direct interactions. ^{40}Ca is known to be a collective vibrational nucleus (Tam56) characterized by vibrational levels at relatively low incident neutron energies. These collective interactions are also discussed elsewhere in this note.

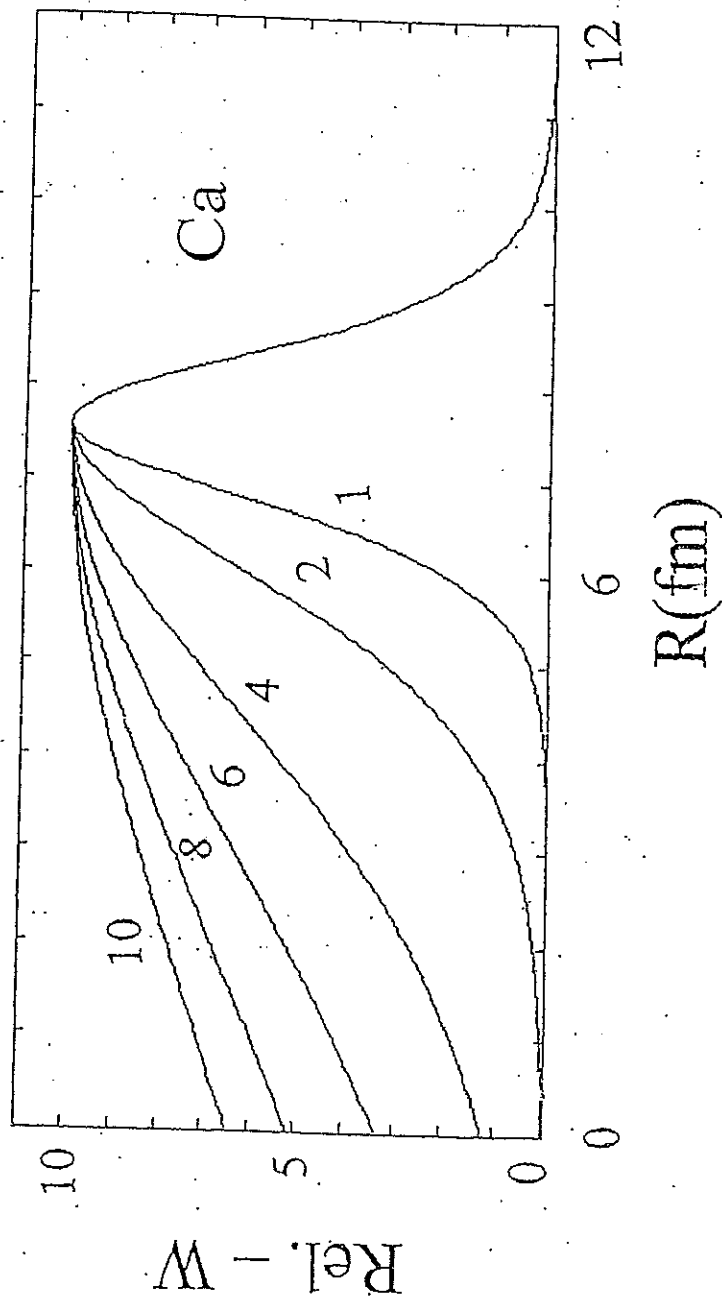


Fig. III.1.1. Relative surface-absorption potential forms as a function of radius obtained with the diffuseness b_{wi} interior to the imaginary radius increasing from 1 to 10 times that of the diffuseness exterior to the imaginary radius. These results correspond to $ASYM = 1, 2, 4, 6, 8, \text{ and } 10$ of Eq. II.2.1, as numerically noted in the figure.

III.2. (n,p) and (n, α) processes

^{40}Ca has among the largest (n,p) and (n, α) cross sections at low few-MeV energies of all the naturally occurring isotopes (NDS). There have been some scattered measurements of them up to several tens of MeV, but the evaluated file systems seem primarily to rely on model calculations. The present considerations assume the (n, α) and (n,p) reactions of ENDF/B-VII. These seem reasonably consistent with what corresponding experimental information that is available (Her). ENDF/B-VII appears to actually be JEFF-3, which is an evaluation by Koning and coworkers (A. Koning, NRG Petten). It seems largely based upon calculations using the TALYS model-code system. The resulting evaluated results are shown in **Fig. III.2.A**. In the present application we make the simple assumption of compound nucleus (n,p) and (n, α) processes. This is doubtless an over simplification as various forms of direct interactions may be contributing factors but these will be predominantly at higher energies where many other compound-nucleus channels are open and it is reasonable to assume that neutron compound-nuclei contributions are deleted to negligible values (see. Ref. ALICE)

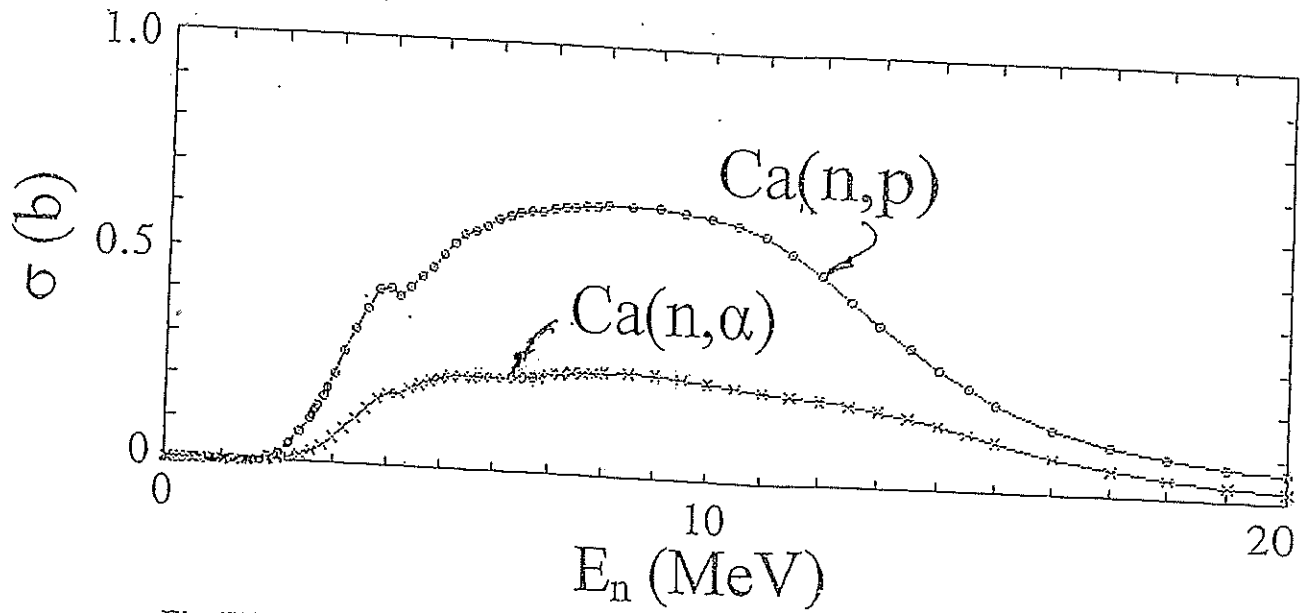


Fig. III.2.A. $Ca-40$ (n,p) (circular symbols) and (n, α) (cross symbols) cross sections taken from ENDF/B-VII. Symbols are the ENDF values which are joined by curves.

III.3. The dispersion relationship

There is a well-known dispersion relationship coupling real and imaginary portions of optical and/or coupled-channels potentials and reflecting causality (Sat83). This relation was considered in the present work as ignoring it would lead to physically questionable results as reported in the literature (Hon+86), (DT88). In the present work the approximate dispersion relationship as defined in ref. LS01 is used. That formulation is simple and well documented in the reference, including a simple computational formalism for implementing the concepts. In that method the dispersion relationship is expressed in the form

$$J(E) = J_{\text{HF}}(E) + (1/\pi) \cdot P \int (J_{\text{W}}(E')/(E-E')) dE', \quad (\text{III.3.1})$$

where $J(E)$ is the total real-potential strength, $J_{\text{HF}}(E)$ is the local equivalent Hartree-Fock strength, $J_{\text{W}}(E)$ is the imaginary potential strength, "P" denotes the principle value of the integral which is taken from $-\infty$ to $+\infty$. The concepts are based upon strengths expressed as volume-integrals-per-nucleon (i.e. J). The application of the concepts requires the specification of potential geometry as discussed below. The integral of Eq III.3.1 can be broken into a surface, $\Delta J_{\text{sur}}(E)$, and a volume, $\Delta J_{\text{vol}}(E)$, components, where

$$\Delta J_{\text{sur}}(E) = (1/\pi) \cdot P \int (J_{\text{sur}}(E')/(E-E')) dE' \quad (\text{III.3.2})$$

and

$$\Delta J_{\text{vol}}(E) = (1/\pi) \cdot P \int (J_{\text{vol}}(E')/(E-E')) dE' \quad (\text{III.3.3})$$

and $J_{\text{sur}}(E')$ and $J_{\text{vol}}(E')$ are surface- and volume-imaginary strengths, respectively, and the integrals are again from $-\infty$ to $+\infty$. Clearly,

$$J(E) = J_{\text{eff}}(E) + \Delta J_{\text{sur}}(E) \quad (\text{III.3.4})$$

where $J_{\text{eff}}(E) = J_{\text{HF}}(E) + \Delta J_{\text{vol}}(E)$. To apply the above concepts one must evaluate the above integrals and convert them to potential parameters assuming appropriate potential geometries. Complex approximations can be found in the literature involving a number of assumptions. What is used here, and in ref. LS01, is a refinement of a simple approach outlined more than a decade ago (LGS78). Combined with reasonable assumptions as to the potential energy dependent forms, the dispersive contribution to the neutron reactions can be relatively easily calculated and applied to the spherical optical model calculations using a recent version of the computer code ABAREX (LS98) (Smi99). This code makes explicit provision for including dispersive effects as derived from the present calculations and the method defined in ref. LS99. The same calculated dispersive parameters can be introduced into a modified version of the coupled channels code ECIS ((Ray96). The above cited assumptions and procedures extend to incident energies of 40 MeV. They may or may not be valid at higher energies.

It is assumed that the imaginary potential is symmetric about the Fermi Energy, E_F , herein given as an absolute value in MeV, taken to be -12 MeV for ^{40}Ca in the laboratory coordinate system (JLM77). It was further assumed that the energy dependence of the surface imaginary parabolic form from $-2E_F$ to zero laboratory energy takes a simple parabolic form, symmetric about $-E_F$ and with a zero magnitude at $-E_F$. Over the same energy range the volume imaginary potential is taken to be zero. From zero energy up to 22 MeV the imaginary potential was assumed to be the imaginary surface potential which was assumed to increase linearly with energy as more channels open. Concurrently the volume absorption remains zero to 22 MeV, and the experimental information at higher energies is too fragmentary and uncertain for firm identification of volume absorption to at least 40 MeV. However, some “global” models consider volume absorption at very low energies (WG86). At much higher incident energies the volume absorption is certainly prominent, but the details of the transition from surface to volume absorption are obscure. It must be a smooth energy dependant transition of the geometry, not the separate volume and surface components usually encountered in the literature. The details of this energy-dependent transition is further discussed below. From 22 MeV the surface absorption strength was assumed to fall linearly with energy to a zero value at 100 MeV. These energy-dependent variations of the imaginary strengths are illustrated in ref. LS99. They are a reasonable physical representation. However, other linear and non-linear representations can be used if one can reasonably justify them. Various alternatives that were explored led to similar results.

With the above approximations one can use the methods of ref. (LS01), to calculate the various dispersive strengths. The calculations were carried out in an iterative manner, repeating the fitting of the experimental information with a given model several times until the dispersion contributions reasonably converged to stable values. The total ($\Delta J_T = \Delta J_V + \Delta J_S$), volume (J_V) and surface (J_S) dispersive strengths calculated using the DOMA potential are illustrated in **Fig. III-3-1**. The J_{HF} and $J_{HF} + \Delta J_V$ are both essentially linear functions of the energy and not distinguishable from experimental interpretation. The common experimental interpretation leads to J_{HW} energy dependencies as no account has been taken of the volume dispersion contributions. The surface dispersion contribution, ΔJ_W , starts as a significant component at zero energy and then decreases to negative values at 40 MeV. All dispersive contributions are zero at $-E_F$ at which energy there is a symmetrical inversion of the dispersion contributions with energy. Similar results are obtained with alternate dispersive models.

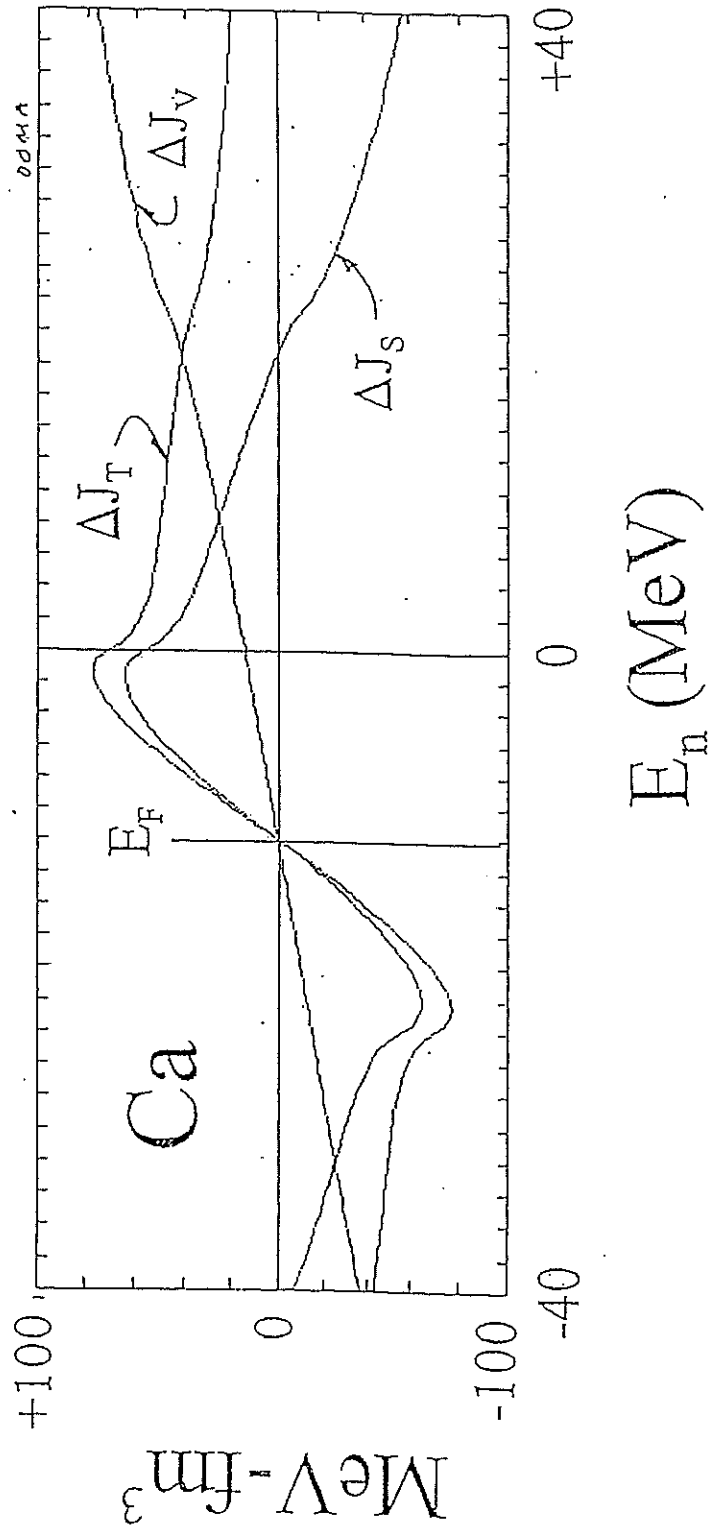


Fig. III.3.1. Contributions from the dispersive integrals ΔJ_{sur} and ΔJ_{vol} of Eqs. 2 and 3 as a function of energy and the total of the two $\Delta J_T = \Delta J_{\text{sur}} + \Delta J_{\text{vol}}$. These illustrative calculations are based upon the DOMA potential outlined above.

The application of the above dispersion contributions to model interpretations requires the conversion to a specific geometric form. Throughout these considerations it was assumed that the real potentials are the Saxon-Woods form and the imaginary potentials the Saxon-Wood-Derivative form (Hod94). Furthermore, volume dispersive and real potentials were assumed to have the same geometries, as were the surface dispersive and imaginary potentials. With these assumptions, the relations between strengths in terms of volume-integrals-per-nucleon and potential magnitudes are defined by well known formulas which are, indeed, a part of the ABAREX spherical optical-model-code. With these assumptions, the formalism of ref.(LS01) provides the fraction of the surface-imaginary potential that dispersive effects add to the real potential and the similar total-dispersive fraction. As noted above, only the surface contribution can be identified by experimental interpretation. Its geometry will be the same as that of the energy dependent imaginary potential, and it may be a positive or negative contribution depending on energy. These energy dependent dispersive contributions are illustrated in **Figs. III.3.1** and **III.3.2**. They can be implemented in a spherical optical-model interpretation using the code ABAREX which makes explicit provision for the use of the surface-dispersion via the input subroutine "DISP" (LS01, LS98 and Smi99). The same result can be obtained in the coupled-channels calculations using the code ECIS96 (and other codes) by adding an appropriate surface term to the real Saxon-Woods potential.

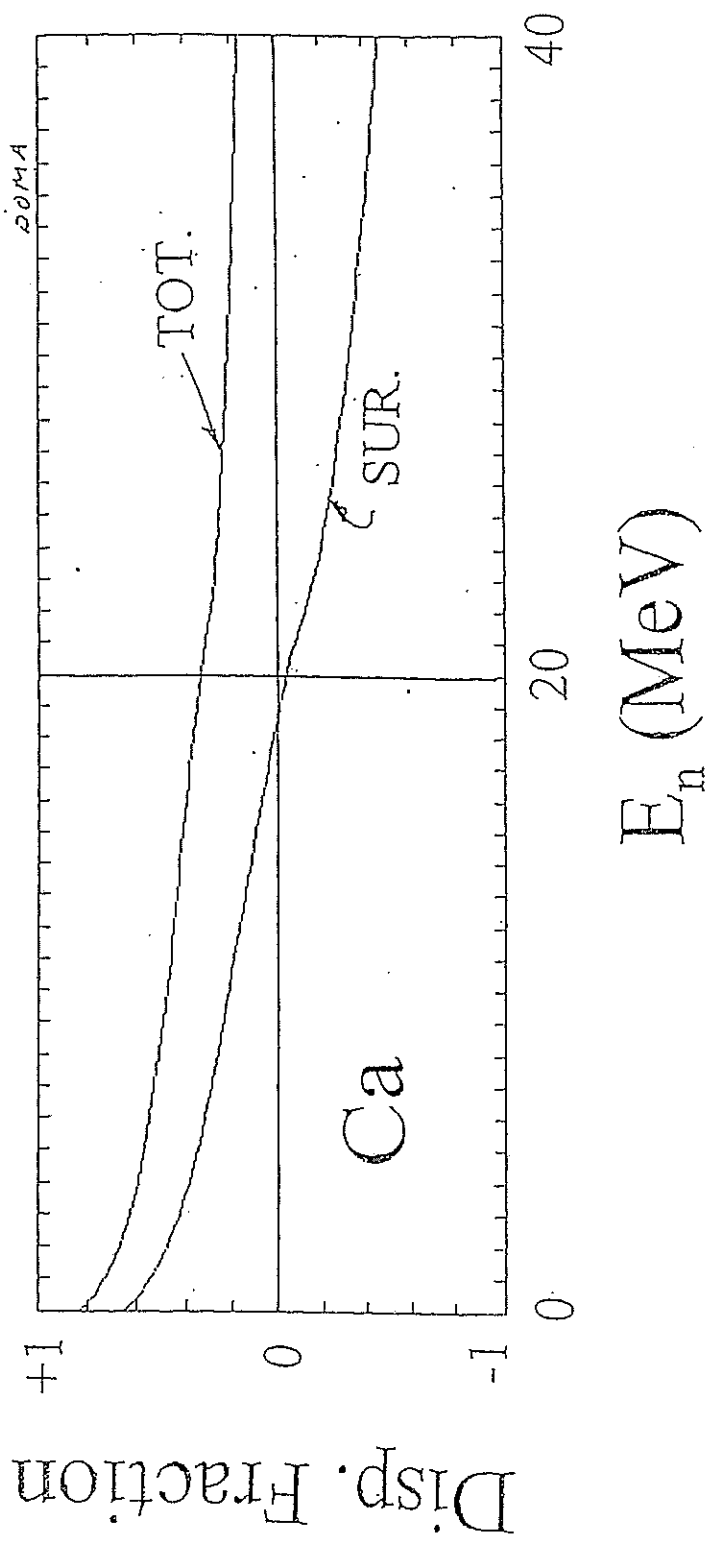


Fig. III.3.2. The dispersive fraction of the imaginary potential that is added to the real potential. SUR denotes the surface contribution and TOT the total contribution consisting of surface and volume contributions. This illustration is deduced from the DOMI discussed above.

IV. Experimental Interpretation and Fitting

All of the experimental interpretations of this work and many of the physical conclusions are based upon extensive least-square fitting using the spherical, dispersive, asymmetric and vibration models outlined above and the experimental neutron data available in the literature up to incident energy of 40 MeV. As outlined above, there is little higher-energy experimental differential scattering information and it is largely concentrated at very forward scattering angles. The interpretations varied from simple SOM fitting of the elastic scattering data to comprehensive considerations including compound-nucleus processes due to np and n α processes, the total cross sections, and dispersion and asymmetry effects, and inelastic-scattering processes. The large data base included 82 differential elastic distributions and many hundred total cross sections. All of the fitting varied the six parameters, real and imaginary strengths, radii and diffuseness at each step. Spin-orbit potentials were kept fixed to those of reference (WG85). For each case the fitting started with six parameter fitting, from which the real diffuseness was determined. Then five parameter fitting was used to determine the real radius, followed by four parameter fitting from which the imaginary radius was fixed, then three parameter fitting was used to set the imaginary diffuseness. Then two parameter fitting from which the real potential strength was determined, and finally one parameter fitting determined the imaginary strength. These six steps were pursued through each of the 82 incident energies and the cycle was iterated at least three times for each potential to obtain the final parameter set. These fitting cycles were followed through for each of the choices of models extending from the simple SOM to complex vibration coupled-channels models, including dispersion effects, asymmetric surface absorption and consideration of the effect of (n,p) and (n, α) processes. All together there were more than several hundred such sets of fitting cycles and resulting potentials that provided physical descriptions of various qualities as discussed below. These results are outlined in the following subsections.

IV.1. The Conventional Spherical Optical Model

Table IV.1.1. Parameters of a detailed fit to Ca data using the conventional SOM ABAREX model with no dispersion nor (n,p) or (n, α) compound nucleus reactions, nor any imaginary potential asymmetry. The parameters are those of "Potential 40".

Real Potential parameters

$$\text{Depth, } V=54.742-1.3505 \cdot E+0.070124 \cdot E^2-0.001104 \cdot E^{**3} \text{ (MeV)}$$

$$\text{Radius, } r_v=1.2820-0.004198 \cdot E-0.000006109 \cdot E^{**2} \text{ (fm)}$$

$$\text{Diffuseness, } a_v=0.34507+0.30966 \cdot E-0.00057428 \cdot E^{**2} \text{ (fm)}$$

$$\text{Strength, } J_v=489.66-5.4226 \cdot E+0.36874 \cdot E^{**2} \text{ (MeV/fm^{**3})}$$

Imaginary Potential parameters

$$\text{Depth, } W=0.97574+0.25241 \cdot E+0.017290 \cdot E^{**2}-0.00082572 \cdot E^{**3} \text{ (MeV)}$$

$$\text{Radius, } r_w=1.2669 \text{ (fm)}$$

$$\text{Diffuseness, } a_w=1.1584-0.043596 \cdot E+0.00079668 \cdot E^{**2} \text{ (fm)}$$

$$\text{Strength, } J_w=31.359+8.7954 \cdot E-0.28686 \cdot E^{**2}+0.0029637 \cdot E^{**3} \text{ (MeV/fm^{**3})}$$

Spin-Orbit Potential parameters (WG85)
 Depth, $V_{so}=5.767-0.015 * E$ (MeV)
 Radius, $r_{so}=1.103$ (fm)
 Diffuseness, $a_{so}=0.5600$ (fm)

IV.2. Asymmetric Absorption

Table IV.2.1. Parameters resulting from a detailed 6-parameter spherical optical-model fit through 3 cycles with the $ASY=1+0.4 * E$, and (n,p) and (n,alpha) contributions from ENDF-VII. The total cross section weight was 10. 13 excited levels were used up to 6.038 MeV with Gilbert and Cameron (GC65) statistical representation of higher lying levels. All the calculations used the ABACN version of the ABAREX model code (LS99). The parameters are those of Potential 93.

Real Potential Parameters

Depth, $V=57.802-1.1140 * E+0.056659 * E^2-0.0009843 * E^3$ (MeV)
 Radius, $r_v=1.264-0.01076 * E+0.000011872 * E^2$ (fm)
 Diffuseness, $a_v=0.3249+0.09884 * E-0.006464 * E^2+0.0001779 * E^3-0.000001784 * E^4$ (fm)
 Strength, $J_v=511.8-0.2025 * E-0.1893 * E^2+0.002286 * E^3$ (MeV/fm³)

Imaginary Potential Parameters

Depth, $W=3.4314+1.6085 * E-0.14531 * E^2+0.00460 * E^3-0.00005042 * E^4$ (MeV)
 Radius, $r_w=1.4496+0.008752 * E-0.000254 * E^2$ (fm)
 Diffuseness, $a_w=0.1796-0.0082224 * E+0.0004885 * E^2-0.00002353 * E^3$ (MeV)
 Strength, $J_w=34.697+74.024 * E-5.2202 * E^2-0.1601 * E^3-0.001764 * E^4$ (MeV/fm³)

Spin-Orbit Potential Parameters (as per reference (WG85), and Table IV.1.1))

IV.3. Dispersive Effects

Dispersive effects were given detailed consideration using the concepts, parameters, potential assumptions and methods of Lawson and Smith, as defined in detail in reference (LS01), and only in the context of spherical optical-model calculations. They were not considered in the deformed vibrational calculations and interpretations. Other physical effects, such as asymmetric imaginary potentials, had a far greater impact on the physical results and masked any dispersive effects.

IV.4. Vibrational Coupling

Table IV.4.1. Parameters resulting from a detailed fit to the Ca data using a two level ECIS vibrational model with no asymmetric absorption nor (n,p) and/or (n,alpha) contributions or dispersive contributions. Levels, deformations and spin-orbit potential are as give by Honre et al. (Hon+86). The fitting went through six cycles using ANLECIS. The real potential was of the Saxon-Woods form and the imaginary potential of the Saxon-Woods-Derivative form.

Real Potential

$$\text{Depth, } V=52.996-1.1031 * E+0.07007 * E^2-0.0012806 * E^3, \text{ MeV}$$

$$\text{Radius, } r_v=1.3705-0.016584 * E+0.00029369 * E^2, \text{ fm}$$

$$\text{Diffuseness, } a_v=0.22243+0.099017 * E-0.004865 * E^2+0.00006650 * E^3, \text{ fm}$$

Imaginary Potential

$$\text{Depth, } W=5.4668+0.68098 * E-0.036475 * E^2+0.0005118 * E^3, \text{ MeV}$$

$$\text{Radius, } r_w=1.4115-0.008980 * E-0.00009252 * E^2, \text{ fm}$$

$$\text{Diffuseness, } a_w=0.1267+0.02417 * E-0.00021828 * E^2, \text{ fm}$$

Spin-Orbit Potential of Walter and Guss (WG85)

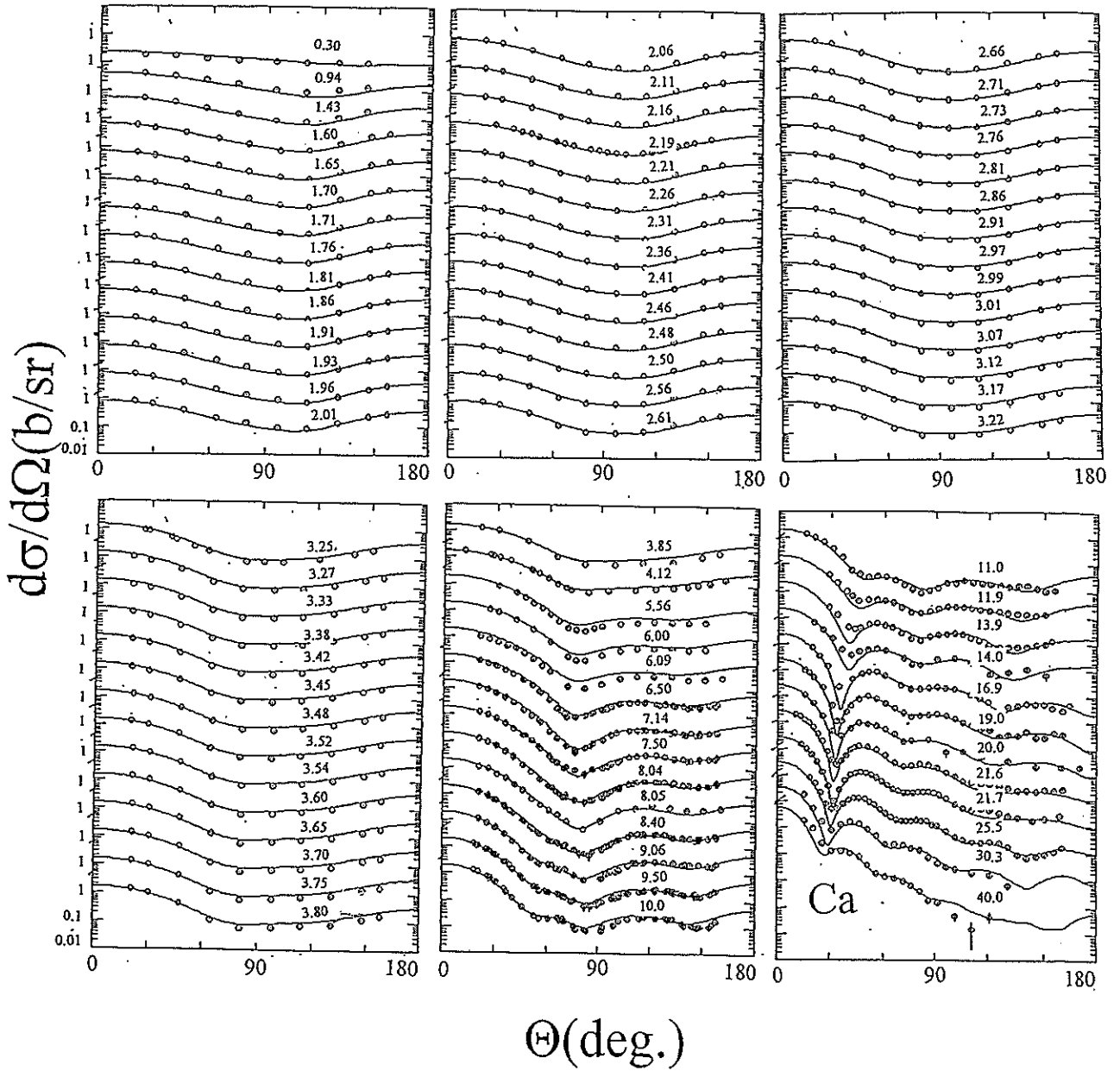


Fig. IV.4.1. Comparisons of measured neutron differential elastic scattering cross sections (circular symbols) with results calculated using an ECIS vibrational program with no imaginary potential asymmetry, dispersion nor (n,p) and/or (n,α) effects (curves) (potential 103). Average incident neutron energies are numerically noted. These experimental distributions are the same as used in the spherical optical-model interpretations.

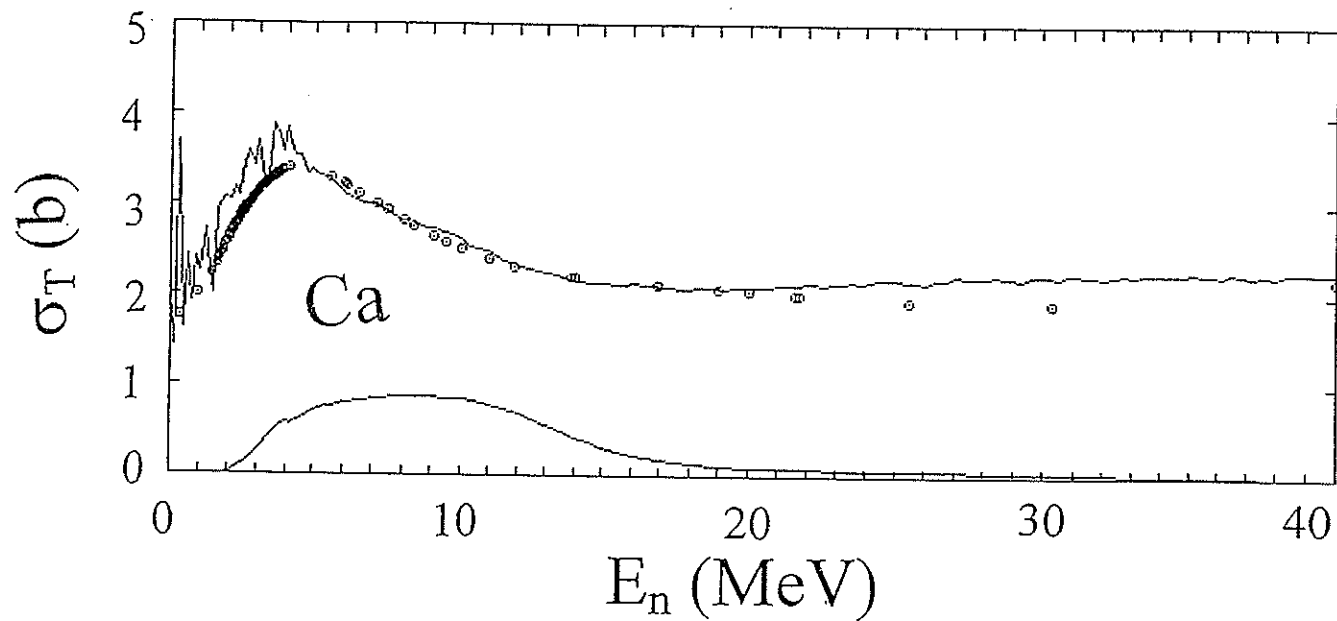


Fig. IV.4.2. Total Ca total cross sections calculated from the fitting of the vibration potential of potential 103 (circular symbols) compared with the total cross sections of the averaged experimental data base (solid curve). Also indicated by a solid curve is the sum of (n,p) and (n,alpha) cross sections as given in ENDFVII.

IV.5. (n,p) and (n, α) Effects

All of the (n,p) and (n, α) contributions were taken from ENDFVII. Some of the fits used the full ENDFVII values, assuming that these two reactions were entirely compound-nucleus processes. In other cases the input (n,p) and (n, α) values were reduced from the ENDFVII values. The fitting results indicated little contribution from these two reactions. Thus these reactions must largely be due to some reaction mechanism other than compound-nucleus processes. This is not surprising as these charge-particle emission processes are likely largely, if not entirely, due to some type of direct-reaction processes. These are dealt with in a number of calculation codes, for example ALICE (ALICE, M. Blann) ,GNASH (GNASH, P. Young) or (TALYS, A. Koning et al.)

Acknowledgements

Throughout this work the author is very much indebted to Dr. Steven J. Grammel for his technical assistance, particularly in the area of computer software. Without his detailed assistance much of this work would not have been possible.

References

- (ALICE) Nuclear reaction code, version 2010, M. Blann, private communication.
- (DT) J. Delaroche and Tornow, *Phy. Let.*, B 203 4 (1988).
- (Elt61) L. Elton, *Rev. Mod. Phys.* 30 557 (1958), also *Nuclear Size*, Oxford Univ. Press (1961).
- (ENDF) ENDF/B-VII, Evaluated Nuclear Data File B., Version VII. Evaluated Nuclear Data Center, Brookhaven National Laboratory.
- (EV78) P. Endt and C. Van de Leun, *Nucl. Phys.* A310 561 (1978).
- (Fes58) H. Feshbach, *Ann. Rev. Nucl. Sci.* 8 49 (1958).
- (FPW54) H. Feshbach, C. Porter and V. Weisskopf, *Phys. Rev.* 96 448 (1954).
- (GC65) A. Gilbert and A. Cameron, *Can. J. Phys.* 43 1446 (1965).
- (GNASH) Nuclear reaction code, version 2008, P. Young, private communication.
- (GPT68) G. Greenlees, G. Pyle and Y. Tang., *Phys. Rev.* 171 1115 (1968), and *Phys. Rev. C* 1 145 (1970).
- (Her08) H. Herman, private communication 2008.
- (Hjo+45) E.Hjort et al., *Phys. Rev. C* 50 2751 (1945).
- (Hod63) P. Hodgson, *The Optical Model of Elastic Scattering*, Oxford Press (1963).
- (Hod94) P. Hodgson, *The Nucleon Optical Model*, World Scientific, Singapore (1994).
- (Hon+86) G. Honore et al., *Phys. Rev. C* 33 1129 (1986).
- (HWJ69) B. Holmqvist, T. Wiedling and , S. Johansson, Report AE-366 (1969).
- (JLM77) J. Juekenne, A. Lejeune and C. Mahaux, *Phys. Rev. C* 16 80 (1977).
- (KP74) W. Kinney and F. Perey, Report ORNL-4909 (1974).
- (Kon97) A. Koning NRG Petten.
- (KD03) A. Koning and J. Delaroche, *Nucl. Phys. A* 713 231 (2003).
- (Kon+07) A. Koning et al., *Proc. Inter. Conf. on Nucl. Data for Sci. and Technology*, EDP Sciences, p.211 (2008).
- (Lan+59) A. Lane, J. Lynn, E. Melkonian and E. Ray, *Phys. Rev. Lett.* 2 424 (1959).
- (Lan62) A. Lane, *Nucl. Phys.* 35 676 (1962).
- (LGS78) R. Lawson, P. Guenther and A. Smith, *Phys. Rev. C* 36 1298 (1987).
- (LS99) R. Lawson and A. Smith, Argonne Natl. Lab. Reports ANL/NDM-145, and ANL/NDM-147 (1999).
- (LS01) R. Lawson and A. Smith, Argonne Natl. Lab. Report ANL/NDM-152 2001).
- (MN81) C. Mahaux and N. Ngo, *Phys. Lett B* 100 285 (1981).
- (Mol80) P. Moldauer, *Nucl. Phys. A* 344 185 (1980).
- (Mug06) S. Mughbghab, *ATLAS of Neutron Resonances*, Elsevier, Amsterdam (2006).
- (NNDC) National Nuclear Data Center, Brookhaven National Laboratory, Upton, New York.
- (NDS) Nucl. Data Sheets, Brookhaven National Laboratory.
- (Ols+82) N. Olson et al., *Nucl. Phys.* 385 285 (1982).
- (Ols+82) N. Olsen et al., *Nucl. Phys. A* 388 288 (1982).
- (OR82) N. Olsen and E. Ramstrom, *Nucl. Phys. A* 388 288 (1982).
- (Osb+04) J. Osborn et al., *Phys. Rev. C* 70 0554613 (2004).
- (Pig+81) M. Piganelli, H. von Geramb and R. De Leo, *Phys. Rev. C* 24 369 (1981).
- (Rap82) J. Rapaport, *Phys. Reports* 87 25 (1982).
- (Ray96) J. Raynal, CEA Report-N-2772 (1996), and private communication.

- (Sat83) G. Satchler, Direct Nuclear Reactions (1983), Addison-Westley, Reading, MA.
- (Smi07) A. Smith, Argonne National Laboratory Report ANL/NDM-163, and Ann. Nucl. Energy, 35 890 (2008).
- (TALYS), Nuclear Reaction Code. A. Koning et al., 2008).
- (Toe74) R. Toepke, Report KFK-2122 (1974) #20574.
- (Tor+82) W. Tornow et al., Nucl. Phys. A 385 373 (1982).
- (Wol51) L. Wolfenstein, Phys. Rev. 82 690 (1951).
- (WG85) R. Walter and P. Guss, Conf. on Nuclear Data for Basic and Applied Science, (1985), Gordon and Breach, editors P. Young et al.